Chen, B., Liu, S., Liu, J., Jiang, N., and Chen, Q. 2021. "A new wall function for indoor airflow with buoyancy effect," *Building and Environment*, 202: 108029.

A New Wall Function for Indoor Airflow with Buoyancy Effect

Bingqian Chen[1], Sumei Liu[1,2*] Junjie, Liu[1], Nan Jiang[3], Qingyan Chen[2]

[1]School of Environmental Science and Engineering, Tianjin University, Tianjin 300072, China
[2]School of Mechanical Engineering, Purdue University, West Lafayette, IN 47905, USA
[3]School of Mechanical Engineering, Tianjin University, Tianjin 300072, China

[*]*Corresponding email: smliu@tju.edu.cn*

Keywords: CFD simulation; Turbulence flow; Natural convection; Mixed convection; Wall treatment

ABSTRACT

Convective heat transfer on interior surfaces of building envelope is important for predicting building energy consumption. Buoyancy effect is a key factor affecting the convective heat transfer. Reynolds averaged Navier-Stokes (RANS) models combined with standard wall function are often used to simulate convective heat transfer coefficient of an interior wall. However, since buoyancy effect is not considered in the standard wall function, the convective heat transfer is often underestimated, which in turn will affect the prediction of indoor air velocity and temperature distributions. Some researchers modified standard wall function by adjusting the wall Prandtl number. But, the ad hoc adjustment did not always work and had no physical basis. This investigation developed a new wall function for considering buoyancy effect on heat transfer by adding a buoyancy source term to the Navier-Stokes equation for near-wall region. The source term varied with the ratio of buoyancy and inertia forces and is linear to the logarithm of Richardson number. Then four typical indoor flows were simulated with the new wall function to test its performance. The results show that the predicted profiles of air velocity and air temperature and local Nu number were significantly better than those with the standard wall function. The study concluded that the new wall-function can correctly predict convective heat transfer on an interior wall.

1. Introduction

The prediction of convective heat transfer coefficient on building surface, h_c, plays an important role in simulating energy consumption and evaluating thermal comfort in buildings. Obyn and van Moeseke [1] found that the incorrect h_c prediction would lead to 9.5% and 13.2% errors in the annual cooling and heating load prediction for an office building. Fisher and Pedersen [2] found that incorrect h_c predictions resulted in a 42% error in calculating predicted percentage dissatisfied people for thermal comfort in indoor spaces. The h_c is normally determined by solving Navier-Stokes (N-S) equations near the wall surface for the velocity and

temperature distributions in the boundary layer, and then an empirical formula for h_c can be obtained by fitting the velocity and temperature profiles. Direct numerical simulation (DNS), large eddy simulation (LES) and Reynolds average model (RANS) are the main computational fluid dynamics (CFD) methods used to calculate the velocity and temperature distributions in the boundary layer. Due to limited computing resources, the recommended models in engineering were RANS models [3, 4], such as standard k-ε two equation model for fully developed turbulent flows [5]. However, in the boundary layer near the wall where molecular viscosity is dominant, the flow is transitional and laminar. The turbulence model could not correctly predict the convective heat transfer on a boundary layer. Two methods [6] are available for solving the problem: low Reynolds number turbulence models [7-11] and wall functions [12].

The low Reynolds models require fine meshes in the boundary layer to correctly calculate the drastically changing temperature and velocity gradients. Awbi [13] pointed out that the distance between the first layer of the grid and the wall surface should be less than 0.5 mm. The fine meshes made the time to solve the flow in this area 3 to 300 times longer than that with high-Reynolds-number models [14]. Such calculation cost was still unaffordable in engineering applications.

The wall functions used algebraic equations to connect the viscous sublayer and the flow in the fully developed zone, so that there was no need to solve the N-S equation with very fine grids near a wall, thereby reducing the computational cost. The most used wall function was the standard wall function. It was derived from an isothermal sweeping flat plate flow [12]. However, in a non-isothermal indoor flow, the heat dissipation to air by people, equipment, and radiators generated a strong buoyancy effect on the flow. Since these buoyancy was mainly generated in the boundary layer, they seriously affect the convective heat transfer coefficient h_c on the surface [13, 15]. Those studies found that if the standard wall function was used to calculate h_c, the error between the simulated results and the experiment data could exceed 45% [15] and the errors increase with Ra [15-20]. Therefore, the standard wall function was not accurate.

A simple way to correct the standard wall function for indoor air flow is to change the Prandtl number near a wall. The h_c increases as the wall Prandtl number decreases. In indoor flow, one would underestimate the convective heat transfer on an interior wall because the buoyancy effect was not considered [11]. Zhang et al. [21] adjusted the wall Prandtl number according to the difference between the h_c simulated by CFD and the value from the empirical formulas. But adjusting the wall Prandtl number had problems. First, it lacked universality since this method had no physical basis. When buoyancy varied, the wall Prandtl number also changed. In addition, the velocity and temperature distributions near a wall calculated with the modified wall Prandtl number were not accurate. This is because changing the wall Prandtl number caused the temperature gradient in the boundary layer to rise, which in turn increased the velocity gradient of the boundary layer.

Therefore, some scholars try to develop new wall functions by considering the buoyancy effect

[22-25]. But these modifications were for flows in engines. Although the Ra number in an engine is like that in indoor flow, the Re number is much lower. Thus, the wall functions developed for engine flows are not suitable for indoor flow. Ng et al. [26] and Kiš and Herwig [27] used DNS to simulate natural convection to obtain air velocity and temperature distributions in a boundary layer. However, the Ra number simulated was small at 10^7 so these functions were not suitable for indoor flow. Therefore, the aim of the present study was to develop a new wall function for indoor airflow with a high Ra number.

2. Method

This section shows how we developed a new wall function suitable for indoor flow with buoyancy effect based on the N-S equation. First we reviewed the derivation procedure for the standard wall function. The wall function was derived from Couette flow [12] and the corresponding momentum and energy equations are:

$$\rho u \frac{\partial u}{\partial x} = -\frac{dp}{dx} + \frac{\partial \tau}{\partial y} \tag{1}$$

$$\rho u \frac{\partial H}{\partial x} + \rho v \frac{\partial H}{\partial y} = -\frac{\partial}{\partial y}(q - u\tau) \tag{2}$$

where ρ is the fluid density, u is the velocity in the x direction, ν is the velocity in the y direction, p is the pressure, τ is Reynolds stress, H is enthalpy, and q is heat flux.

Equations (1) and (2) neglect the buoyancy term near the wall and the velocity change in the y direction, and use them to obtain the velocity and temperature wall functions:

$$u^+ = \frac{1}{\kappa}\ln(y^+ + C) \tag{3}$$

$$T^+ = \mathrm{Pr}_t(u^+ + P) \tag{4}$$

where u^+ is dimensionless velocity, y^+ is dimensionless wall distance, κ is Von Karman constant, T^+ is dimensionless temperature, Pr_t is wall Prandtl number, and P and C are empirical terms in the wall function. It can be seen from the expression of the thermal wall function that the dimensionless temperature is only related to the dimensionless velocity and the wall Prandtl number. The wall Prandtl number is a constant in the standard wall function. The dimensionless velocity is only related to the dimensionless wall distance, without considering the effect of buoyancy. Therefore, the standard wall function did not consider buoyancy effect.

Without considering buoyancy effect, the standard wall function would underestimate the convective heat transfer or local Nusselt number, Nu:

$$Nu = \frac{hL}{k} \tag{5}$$

$$h = \frac{q}{T_w - T_\infty} \tag{6}$$

where h is the convective heat transfer coefficient, L is the reference length, k is the thermal conductivity of the fluid, T_w is the wall temperature, T_∞ is fluid free stream temperature. The relationship between T^+ and q is:

$$T^+ = \frac{(T_w - T_P)\rho c_p C_\mu^{\frac{1}{4}} k_P^{\frac{1}{2}}}{q} \tag{7}$$

where T_P is the estimated temperature in the first grid cell, c_p is specific heat of fluid, C_μ is coefficient used in the turbulence mode, k_P is turbulence kinetic energy at the wall-adjacent cell centroid. Substitute Equations (4), (6) and (7) into Equation (5):

$$Nu = \frac{(T_w - T_P)\rho c_p C_\mu^{\frac{1}{4}} k_P^{\frac{1}{2}}}{(T_w - T_\infty)\Pr_t[\frac{1}{\kappa}\ln(Ey^+) + P]}\frac{L}{k} \tag{8}$$

Equation (8) shows how the thermal wall function affects the local Nu number. Taking a hot wall as an example to increase the local Nu number of the wall while maintaining the temperature boundary conditions unchanged, it is necessary to decrease the wall Prandtl number.

To develop a new wall function for a non-isothermal flow from the N-S equation, the Boussinesq approximation is added to the right side of the N-S equation:

$$\rho v\frac{du}{dy} = -\frac{dp}{dx} + \frac{\partial \tau}{\partial y} + \frac{\rho\beta}{c_p}(\overline{H_o} - \overline{H})g \tag{9}$$

where H_o is reference enthalpy. We stipulate that the direction along the flow is the x direction and the direction perpendicular to the flow is the y direction. Integration of Equation (9) along the y direction yields:

$$\rho v u_s = -y\frac{dp}{dx} + \tau - \tau_s + \frac{\rho\beta}{c_p} y(\overline{H_o} - \overline{H})g \tag{10}$$

The subscript s represents the surface. For the convenience of writing, we define

$$m_s = \rho v \tag{11}$$

then

$$\tau = \tau_s + m_s u_s + y\frac{dp}{dx} - \frac{\rho\beta}{c_p} y(\overline{H_o} - \overline{H})g \tag{12}$$

Divide both sides of Equation (12) by τ_s to obtain:

$$\tau^+ = 1 + m^+ u^+ + y^+ p^+ - y^+ T^+ S^+ \tag{13}$$

where $\tau^+ = \frac{\tau}{\tau_s}$, $m^+ = \frac{m_s}{\sqrt{\tau_s / \rho}}$, $T^+ = \frac{(\overline{H_O} - \overline{H})\sqrt{\tau_s \rho}}{-q_s}$, $u^+ = \frac{u_s}{\sqrt{\tau_s / \rho}}$, $y^+ = \frac{y\sqrt{\tau_s \rho}}{\mu_c}$,

$p^+ = \frac{\mu_c}{\sqrt{\tau_s^3 \rho}} \frac{dp}{dx}$, and $S^+ = -\frac{\mu_c q_s \beta g}{c_p \tau_s^2}$.

Applying Newton's internal friction law, $\tau = \mu \frac{du}{dy}$

$$\frac{du^+}{dy^+} = \frac{\tau^+}{\mu^+} = \frac{1 + m^+ u^+ + y^+ p^+ - y^+ T^+ S^+}{\mu^+} \tag{14}$$

According to the theory of mixing length hypothesis, $\mu^+ = \kappa^2 (y^+)^2 \frac{du^+}{dy^+}$, Equation (14) can be changed to:

$$\frac{du^+}{dy^+} = \frac{\tau^+}{\mu^+} = \frac{1 + m^+ u^+ + y^+ p^+ - y^+ T^+ S^+}{\kappa^2 (y^+)^2 \frac{du^2}{dy^2}} \tag{15}$$

Let $m^+ = p^+ = 0$,

$$\frac{du^+}{dy^+} = \frac{(1 - y^+ T^+ S^+)^{\frac{1}{2}}}{\kappa y^+} \tag{16}$$

The analytical solution of Equation (16) is:

$$u^+ = -\frac{2}{\kappa}(-\sqrt{1 - T^+ S^+ y^+} + \frac{1}{2} \ln \frac{1 + \sqrt{1 - T^+ S^+ y^+}}{1 - \sqrt{1 - T^+ S^+ y^+}}) + C \tag{17}$$

where the constant in the velocity wall function C is 0.21.

The near-wall energy equation of the new wall function is based on Equation (2), using a method similar to deriving the new velocity wall function. Namely, integrating Equation (2), making the integrated equation dimensionless, and then applying the Fourier law of heat conduction, we can obtain the new temperature wall function as:

$$T^+ = \frac{1 - \sqrt{1 - 2y^+S^+\sigma_{eff}(u^+ + C_t)}}{y^+S^+} \tag{18}$$

where σ_{eff} is Schmidt number and C_t is the constant of thermal wall function that changes with the indoor Richardson number (Ri):

$$\mathrm{Ri} = \mathrm{Ra}/\mathrm{Re}^2 \tag{19}$$

Note that C_t presented in this paper was determined through data fitting with the experiment from Tian and Karayiannis [28, 29], Cheesewright et al. [30] and Blay et al. [7]. We selected those cases because these three cases had relatively complete databases, especially the velocity and temperature distribution of the boundary layer. With the data, Figure 1 shows the logarithmic relationship between C_t and Ri:

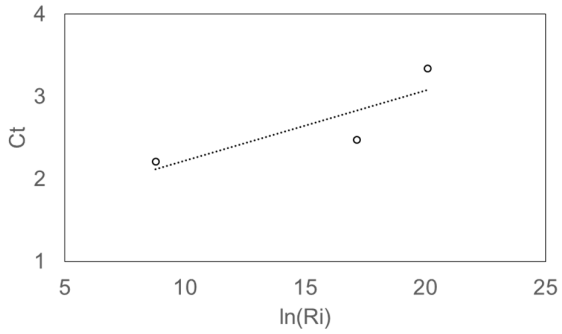

Figure 1. The logarithmic relationship between C_t and Ri.

C_t can be expressed as

$$C_t = 0.085 * \ln(Ri) + 1.37 \tag{20}$$

with R^2 of 0.72.

When the heat flux q increases, the buoyancy and S^+ increase and T^+ decreases. Then the local Nu increases and the convective heat transfer increases. In contrast, the standard wall function would not change no matter how q changes.

This study used the standard k-ε model with the new wall function implemented in ANSYS Fluent commercial CFD program. The numerical scheme for pressure was PRESTO!, and the discretion scheme for momentum, turbulent kinetic energy and turbulent dissipation rate was second-order upwind one. We used a structured grid to speed up the calculation. The number of grids for each case was determined through grid independent solutions. The new wall function evaluation index uses Root Mean Squared Error (RMSE):

$$RMSE = \sqrt{\frac{\sum (x_{\exp} - x_{sim})^2}{n}} \tag{21}$$

where x_{exp} is the measured value, x_{sim} is simulated value, and n is the number of values. The smaller the RMSE means the better performance is.

3. Results

In order to verify the correctness of the new wall function, we used the new wall function to simulate different indoor flows. Indoor flow can be divided into forced, natural and mixed convection. For forced convection that is isothermal flow, the standard wall function can accurately predict the indoor flow so such a flow would not be a subject of this investigation. We focused on indoor natural and mixed convection flows. In order to better reflect the role of buoyancy in the new wall function, we also used the standard wall function with and without the modified wall Prandtl number for comparison. For the convenience of expression, we denoted the standard wall function without modified wall Prandtl number as SWF, the standard wall function with modified wall Prandtl number as MWF, and the new wall function as NWF.

3.1 Natural convection

This study used two natural convection cases from the experiment conducted by Tian and Karayiannis [28, 29] and by Cheesewright et al. [30]. The first case was a two-dimensional case of 0.75 m × 0.75 m with a hot vertical wall on the left and a cold vertical wall on the right as shown in Figure 2(a). The top and bottom walls were well insulated. Since the wall height was only 0.75 m that was smaller than a typical floor height in a building, the temperature difference between the hot and cold walls was increased to have a higher Ra number. Thus, the left wall was 50 °C and the right wall 10 °C. Nevertheless, the corresponding Ra number was only 1.58×10^9 that was still lower than that in a room. Therefore, we selected another case [30] with a height of 2.5 m and a width of 0.5 m as shown in Figure 2(b). The width of this case was much narrower than a room, but it should not have an impact on the convective heat transfer. The temperature of the left wall was 77.2 °C and on the right wall 31.4 °C with a Ra number of 5.0×10^{10}. The dotted lines in Figure 2 represented the locations with measured air velocity, air temperature, and turbulent kinetic energy. The Nu numbers of the hot and cold walls were also measured.

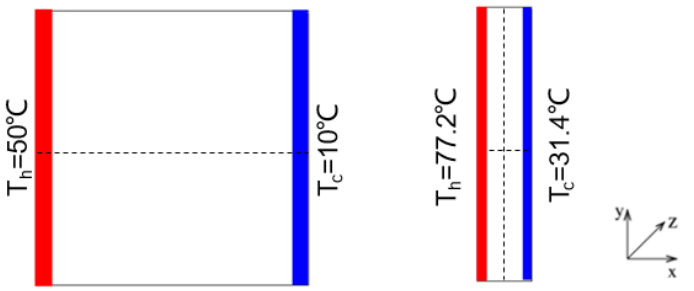

(a) Natural convection with $Ra=1.58\times10^9$ *(b) Natural convection with $Ra=5.0\times10^{10}$*

Figure 2. Two natural convection cases studied.

Figure 3 showed the predicted and measured local Nu number of the hot wall in the first case by Tian and Karayiannis. In the standard wall function, the default value of the wall Prandtl number is 0.85. MWF used different wall Prandtl numbers ranging from 0.15 to 0.75. By reducing the wall Prandtl number, the Nu prediction increased and the simulation error reduced. With Pr_t=0.35, the predicted Nu was closest to the experimental data. If the wall Prandtl number continued to increase, the local Nu was understimated. However, the disadvantage of this method is that one would not know what the correct wall Prandtl number is if there is no experimental data. NWF obtained local Nu prediction that was similar to experimental data.

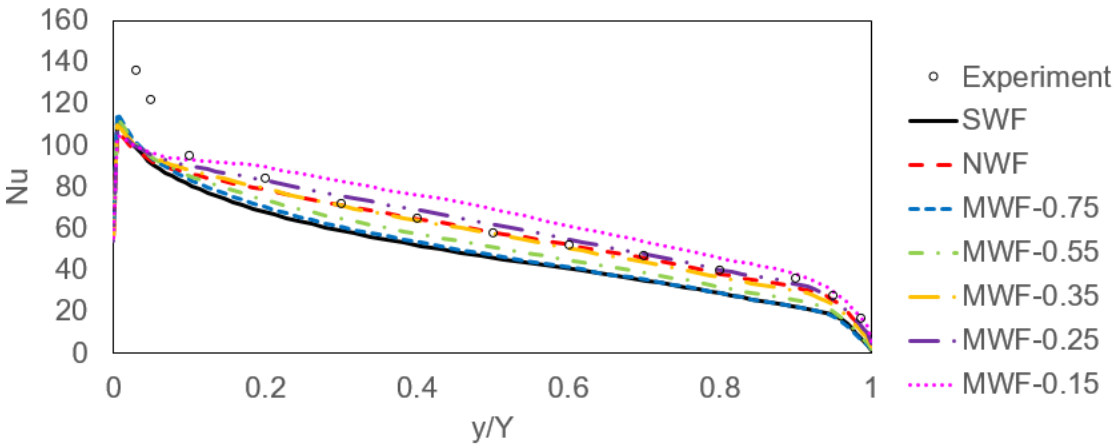

Figure 3. Comparison of predicted and measured local Nu number on the hot wall.

Apart from the need to adjust the wall Prandtl number through experimental data, MWF has another serious defect. Adjusting the wall Prandtl number would cause errors in velocity prediction. Figure 4 showed the predicted and measured V-velocity profiles near the hot wall at Y=0.5. According to the literature, the boundary of differential-heated-convection flow is divided into inner layer and outer layer [31]. In the inner layer, $0\leqslant x/X\leqslant0.0067$, the predicted V-velocity by all wall functions was close to the experimental data. The main difference occurred in the outer layer, $0.0067\leqslant x/X\leqslant0.1$. As the wall Prandtl number increased, the V-velocity predicted by MWF in the outer layer part gradually increased, eventually deviating from the experimental data. In Figure. 3, the Prandtl number calculated by MWF-0.35 agrees the best with the measured data. MWF-0.35 would overestimated the V-velocity in the outer layer. SWF could predict the V-velocity profile while NWF was slightly better.

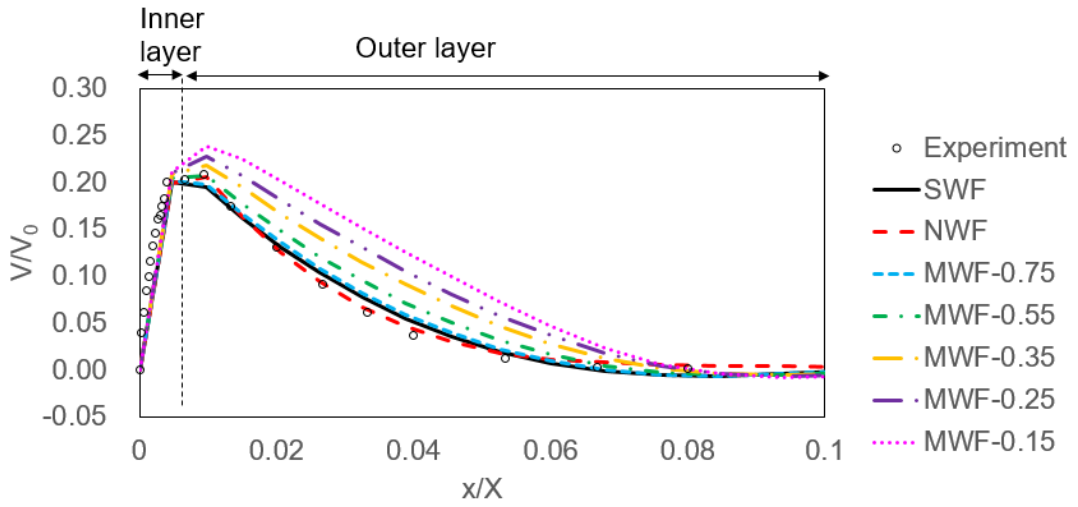

Figure 4. The predicted and measured V-velocity profile near the hot wall at mid-height (Y=0.5).

In differential-heated-convection flow, the temperature in the middle is the mean of the hot and cold surface temperatures regardless the performance of wall functions. However, the temperature profile in the near wall region depends very much on the wall functions. Figure 5 shows the temperature profile near the hot wall in the region of $0 \leqslant x/X \leqslant 0.1$ at y/Y=0.5 height. The position of the first layer grid was at x/X=0.005 as enlarged and embedded in Figure 5. The predicted temperature by MWF and NWF in the first grids was lower than that by SWF. The larger temperature difference between the first grids and hot wall led to a larger the velocity gradient near the wall. This resulted in insufficient velocity attenuation in the outer layer and overestimation of the air velocity. On the other hand, S^+ in NWF was negative so that the first-order derivative of the velocity was larger than that by MWF. Hence, when the NWF modified the thermal wall function, it simultaneously modified the velocity wall function. The velocity attenuation was the same as the experiment. Therefore, NWF can predict accurately air velocity in the outer layer.

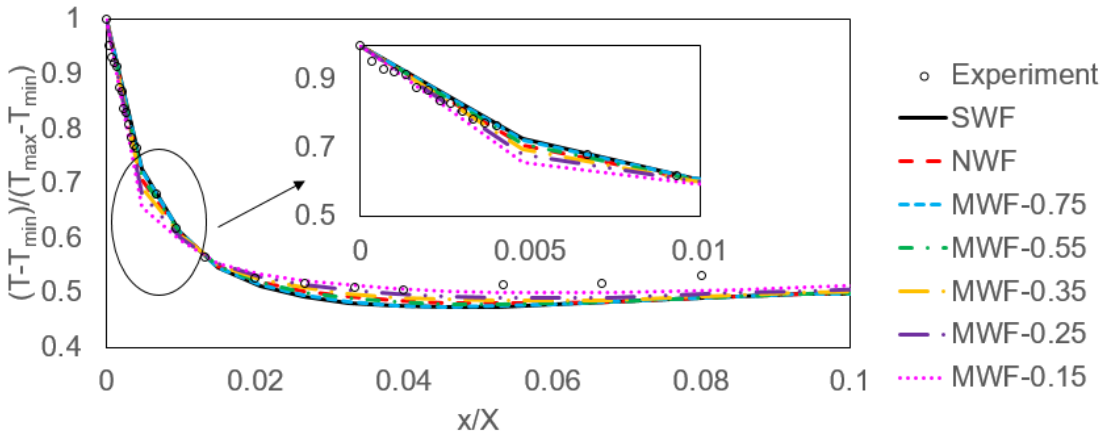

Figure 5. The predicted and measured near wall temperature profiles at the mid-height of the

(Y=0.5).

Figure 6 depicts the velocity fluctuation at Y=0.5. All of the wall functions underestimated the velocity fluctuations. Our NWF did not modify the wall functions for turbulence so it should be surprised to see the similar results. However, the under-prediction of the velocity fluctuation in the model of the cavity was caused by the turbulence model used, namely the standard k-ε model, in all the predictions. The differences on wall functions should not have a major impact in the middle of the cavity.

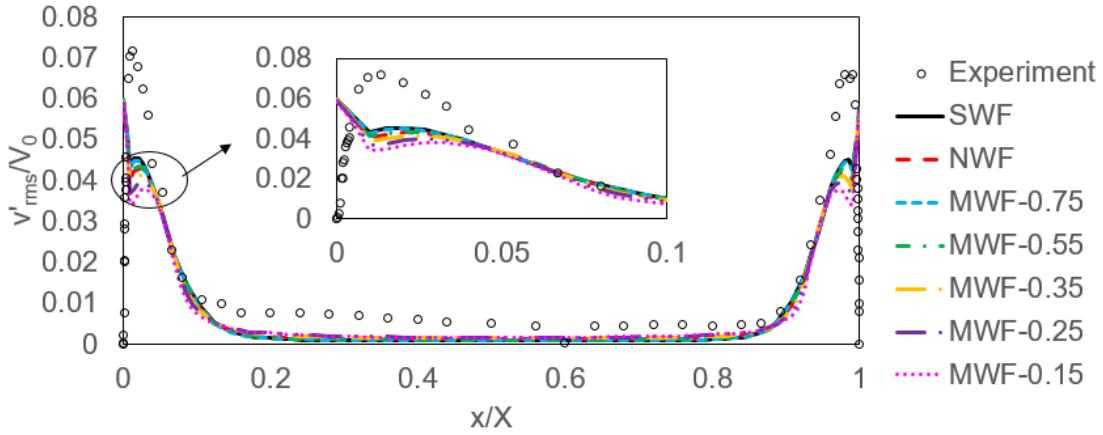

Figure 6. The predicted and measured velocity fluctuation profiles at mid-height (Y=0.5).

Table 3 showed the RMSE values of the three kinds of wall functions in predicting the local Nu number, temperature, velocity, and velocity fluctuations. NWF performed better than SWF in everything except slightly poor in the velocity fluctuations. The performance of MWF depended on the Prandtl number assigned. Without experimental data, it is impossible to guess a correct Prandtl number.

Table 3 RMSE of local Nu, temperature, velocity and velocity fluctuation in the natural convection case of Tian and Karayiannis [28, 29]

	Local Nu	Temperature	V-velocity	Velocity fluctuation
SWF	16.0	0.0367	0.00820	0.0158
NWF	12.9	0.0289	0.00398	0.0184
MWF-0.75	15.5	0.0350	0.01072	0.0161
MWF-0.55	14.0	0.0306	0.01890	0.0169
MWF-0.35	12.7	0.0239	0.03289	0.0183
MWF-0.25	12.8	0.0190	0.04355	0.0194
MWF-0.15	14.4	0.0210	0.05851	0.0147

The performance assessment above was for a lower Ra number than that in buildings. Therefore, we used a second case from Cheesewright et al.[30] for additional validation. Figure 7 illustrates the local Nu number distribution on the hot wall. Again, the predicted local Nu by MWF decreased with the wall Prandtl number. Although Ra in this second case was an order

of magnitude higher than that in the first case, the most appropriate wall Prandtl number in this case was still 0.35. But the local Nu number predicted by NWF was closest to that by MWF-0.55 instead of MWF-0.35. This indicates that the equivalent wall Prandtl number corresponding to NWF was not fixed. The performance of the NWF is acceptable.

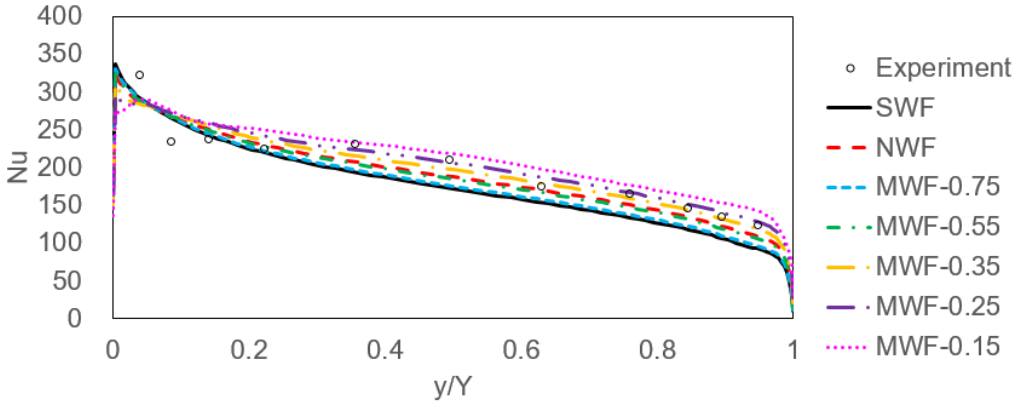

Figure 7 Predicted and measured local Nu number on the hot wall.

Figure 8 shows the V-velocity profile near the wall at y/Y=0.5. The performance of the three kinds of wall functions was again similar. Changing the wall Prandtl number to compensate for the underestimation of convective heat transfer on wall surface would cause an overestimation of the velocity in the outer layer. MWF-0.35 overestimated the V-velocity in the outer layer, compared with SWF. NWF balanced the prediction accuracy of the local Nu and V-velocity and was better than SWF. It was worth noticing that the equivalent wall Prandtl number of NWF was 0.55 for local Nu prediction, but 0.75 in V-velocity prediction. This implies that the equivalent wall Prandtl number of NWF could not be predicted through Ra.

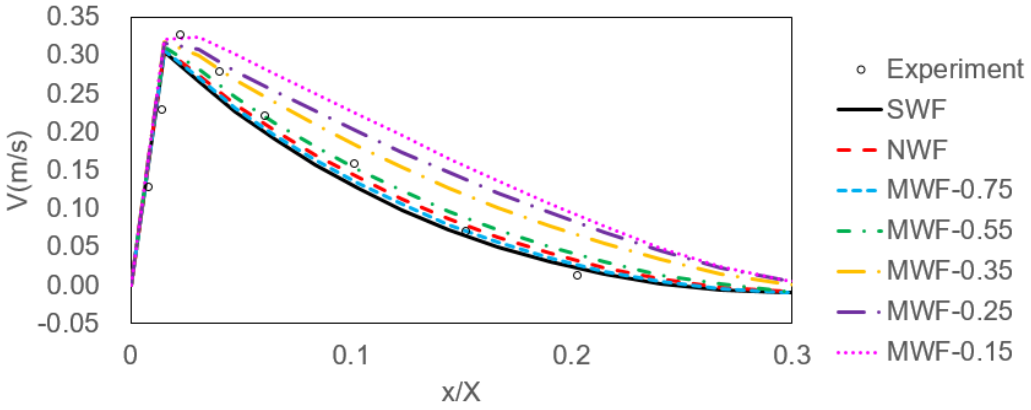

Figure 8 Predicted and measured V-velocity profile near the hot wall at mid-height (Y=0.5).

Due to imperfect insulation, the temperature measured at x/X=0.5 was lower than the average as shown in Figure 9. Therefore, we could only compare qualitatively the temperature trend. In $0.2 \leqslant y/Y \leqslant 0.8$, the predicted temperature profiles by all the wall functions were basically the same and parallel with the experimental one. The slight difference appeared in $0 \leqslant y/Y \leqslant$

0.2 and 0.8≤y/Y≤1. In these two near wall regions, the predicted temperatures of SWF, NWF, MWF-0.75 and MWF-0.55 were similar. However, MWF-0.35, MWF-0.25 and MWF-0.15 gave a higher temperature than NWF and SWF at the bottom and lower temperature than NWF and SWF at the top. Again this demonstrates that NWF can predict accurately heat transfer without sacrificing the accuracy in air temperature prediction.

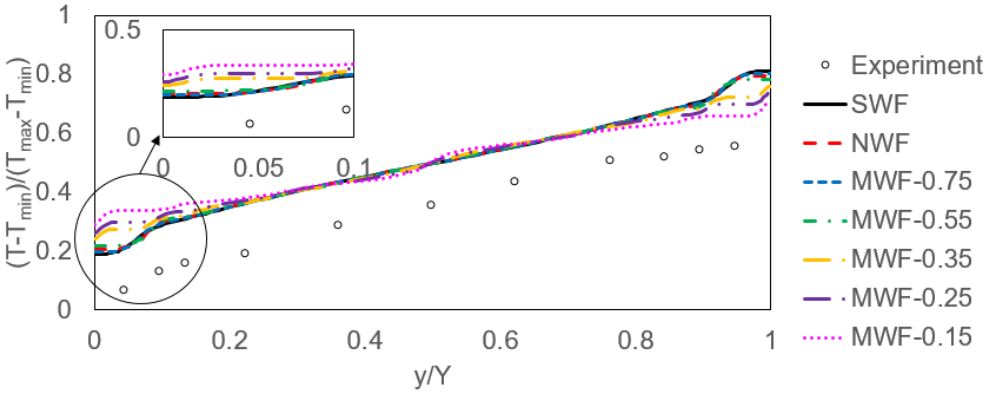

Figure 9 Predicted and measured temperature profiles in the mid-width.

Table 4 showed the RMSE of local Nu number and air velocity calculated with the three wall functions. Clearly NWF did a better job than SWF and the performance of MWF depends on the Prandtl number assigned.

Table 4 RMSE of local Nu number, V-velocity for Cheesewright' case [30]

	Local Nu	V-velocity
SWF	28.5	0.0216
NWF	22.4	0.0167
MWF-0.75	24.3	0.0133
MWF-0.55	20.1	0.0219
MWF-0.35	19.2	0.0428
MWF-0.25	20.2	0.0558
MWF-0.15	24.4	0.0706

The above two cases show that NWF could be used for natural convection flow in indoor spaces. NWF can predict accurately the heat transfer on wall surface and would not distort the air temperature distribution.

3.2 Mixed convection

Mixed convection is with equivalence of inertial force and buoyancy force in buildings. Examples include rooms that use floor radiant heating and make-up air systems in winter and air-conditioning in summer. In view of these two situations, this paper selected a two-dimensional mixed convection case and a three-dimensional mixed convection case to assess the performance of the new wall function.

The two-dimensional mixed convection case was a room with a dimension of 1.04 m × 1.04 m with experimental data from Blay et al. [7] as shown in Figure 10. The floor temperature was 35.5°C but all other surface temperature was 15 °C. The air supply temperature was 15°C with a velocity of 0.57 m/s from the inlet on the top left. The inlet width was 0.18 m and the outlet width 0.24 m.

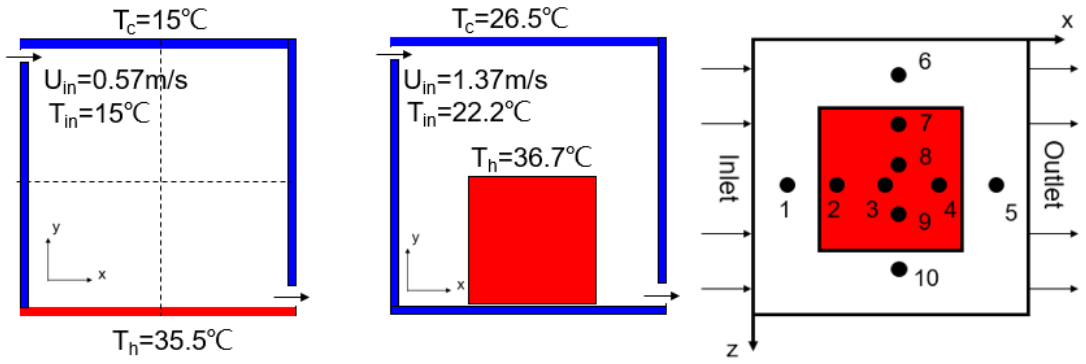

(a) The 2D case *(b) The 3D case (section)* *(c) The 3D case (plane)*

Figure 10. The schematic of the mixed convection cases.

Figure 11(a) showed the U-velocity profile at the mid-width of the cavity (x=0.52 m). In the vertical direction, the heating floor generated strong thermal plumes, so the U-velocity near the floor reached nearly -0.3 m/s. Since buoyancy was not considered, SWF underestimated it by 21.0%. Different from natural convection, in mixed convection MWF further underestimated the velocity and different wall Prandtl numbers had little effect on velocity prediction. NWF gave the best prediction of the plume velocity near the wall. But on the top wall where forced convection was dominated, NWF overestimated the air velocity.

Figure 11(b) showed the V-velocity profile in the mid-height of the cavity (y=0.52 m). The velocity on the right wall predicted by SWF was 22.5% lower and on the left wall was 10.4% lower than the experimental data. This was because the airflow in the room flowed in a clockwise direction, the buoyancy effect on the left wall was stronger than the right wall. The prediction on the left wall by NWF was better than that by SWF, but not clear on the right wall due to limited experimental data point. MWF predicted a lower velocity than SWF on the left wall and almost the same on the right wall.

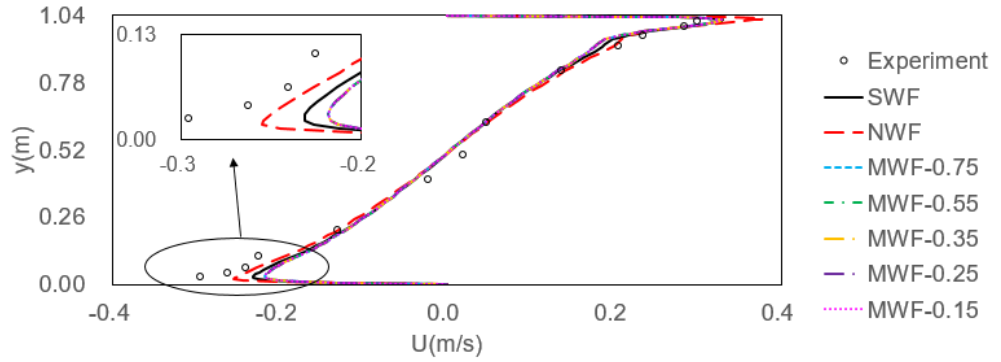

(a) U-velocity profile at the mid-width (x=0.52 m)

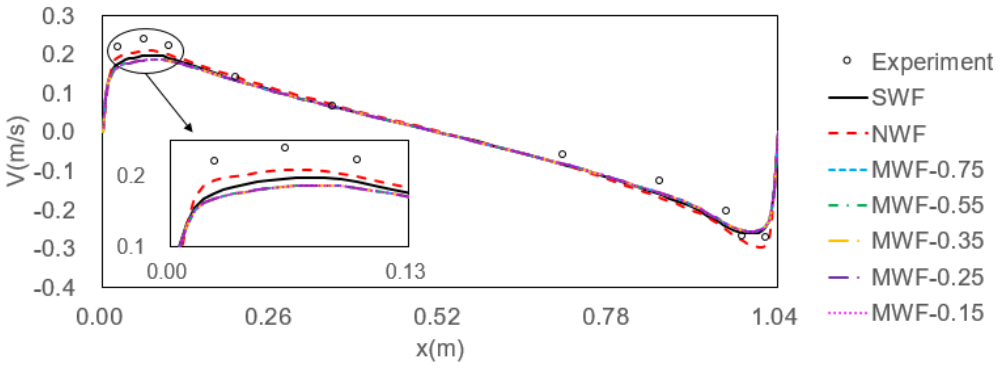

(b) V-velocity profile at mid-height (y=0.52 m)

Figure 11. The predicted and measured air velocity profiles for the two-dimensional mixed convection case.

Figure 12(a) shows the air temperature profile at the mid-width of the cavity (x=0.52 m). In the core region, the predicted temperature by SWF was 1 K lower than the actual one due to underestimation of the convective heat transfer on walls. By adjusting the wall Prandtl number to 0.75, the predicted core temperature rose by 0.4 K. However, continuing to reduce the wall Prandtl number further did not increase much the air temperature. The temperature prediction by NWF was equivalent to MWF-0.15. Because the buoyancy in the core area was not strong, the advantages of NWF were not fully shown. Near the floor with strong buoyancy, NWF performed much better than SWF.

Figure 12(b) depicts the air temperature profile in the mid-height of the cavity (y=0.52 m). The predicted temperature in core area was already discussed above. In the near wall regions, NWF did a better job than SWF and MWF. Since the buoyancy effect in the near wall regions was weaker than that near the floor, the improvements were less evident.

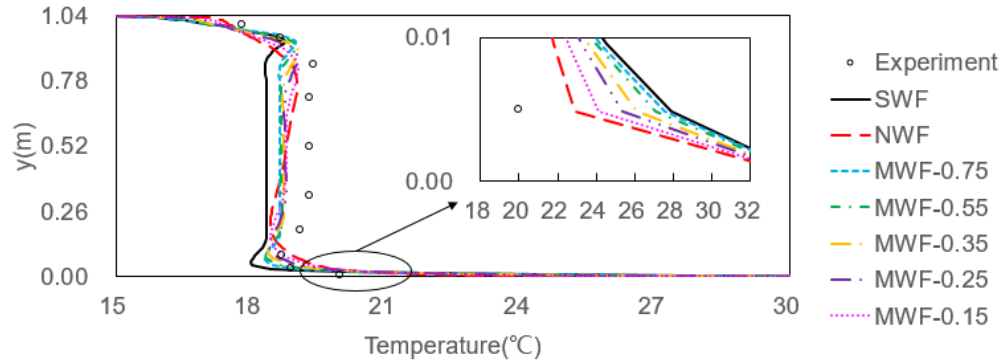

(a) Air temperature profile at the mid-width (x=0.52 m)

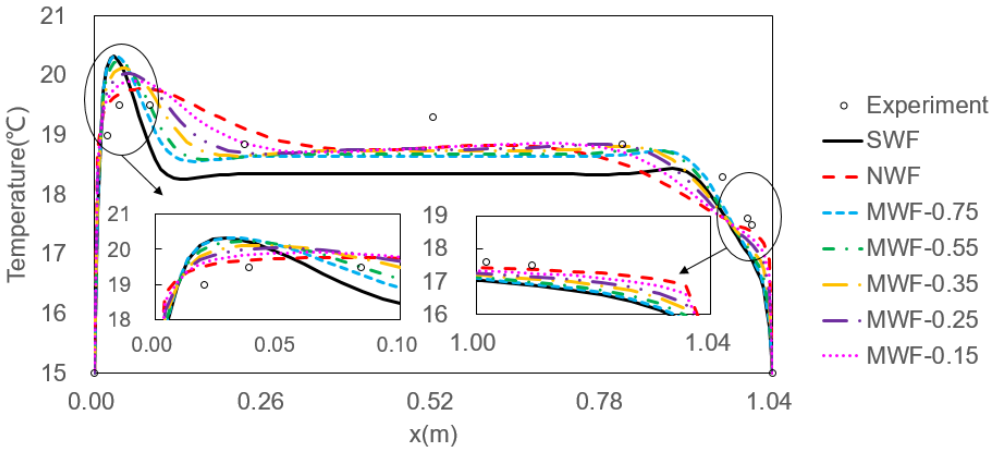

(b) Air temperature profile at mid-height (y=0.52 m)

Figure 12. The predicted and measured air temperature profiles for the two-dimensional mixed convection case.

Figure 13 illustrates the vertical and horizontal profiles of air turbulent kinetic energy. The predicted turbulent kinetic energy by NWF and MWF were slightly higher than SWF, especially near the floor where buoyancy was strong. While near the ceiling where inertia force dominated, the turbulent kinetic energy calculated by NWF was lower than that of SWF. Since the new wall functions were not for turbulence energy, the small differences shown in the figure may not be caused by the wall functions. In the near wall region, the profiles predicted by NWF look different from the others, but the reason was not clear.

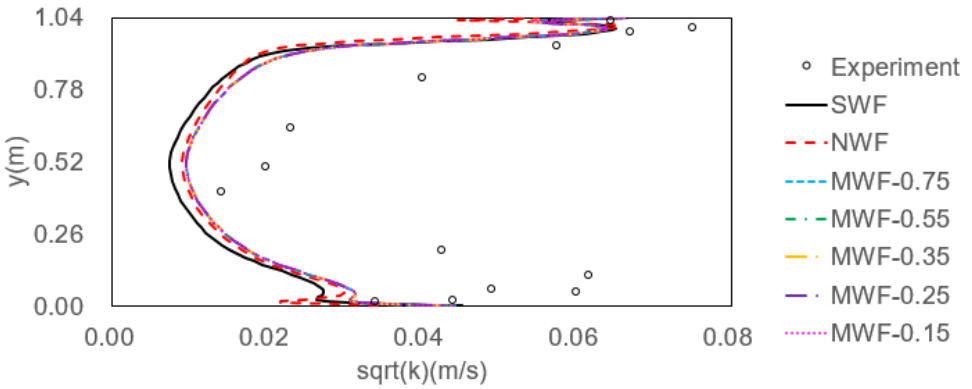

(a) At the mid-width (x=0.52 m)

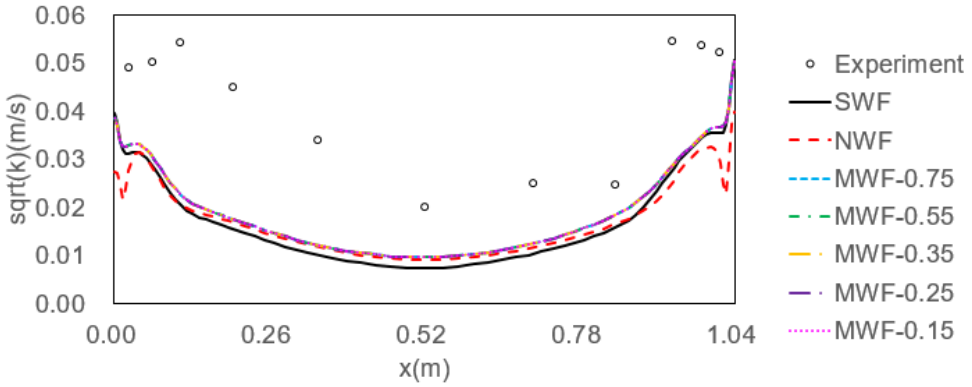

(b) At mid-height (y=0.52 m)

Figure 13. The predicted and measured turbulence kinetic energy profiles for the two-dimensional mixed convection case.

Table 5 showed the RMSE of the air velocity, temperature and turbulent kinetic energy for the three wall functions at the two mid-sections. The RMSE of temperature in horizontal direction was the lowest for NWF and highest for SWF that was well expected. Compared with SWF, the improvement by MWF was rather significant. There were no major differences among the RMSE of turbulent kinetic energy for the three kinds of wall functions.

Table 5 RMSE of air velocity, temperature and turbulent kinetic energy for the two-dimensional mixed convection.

	Vertical direction			Horizontal direction		
	U-velocity	Temperature	Kinetic energy	V-velocity	Temperature	Kinetic energy
SWF	0.0280	2.55	0.0213	0.0296	0.729	0.0216
NWF	0.0247	1.05	0.0216	0.0282	0.384	0.0223
MWF-0.75	0.0339	0.53	0.0193	0.0330	0.607	0.0200
MWF-0.55	0.0339	0.51	0.0193	0.0330	0.554	0.0200
MWF-0.35	0.0339	0.49	0.0193	0.0330	0.496	0.0200
MWF-0.25	0.0339	0.49	0.0193	0.0330	0.460	0.0200

MWF-0.15	0.0330	0.52	0.0193	0.0330	0.409	0.0200

The above cases were all two-dimensional. Actual indoor spaces are always three-dimensional. Therefore, we used a three-dimensional mixed convection case with experimental data from Wang and Chen [32] to further assess the performance of the wall functions. The case was a room with a dimension of 2.44 m × 2.44 m × 2.44 m as shown in Figure 10(b) and the room contained a heated box of 1.22 m × 1.22 m × 1.22 m in the center on the floor. The heated box represented the heat generated by occupants and equipment in the room. The surface temperature of the box was 36.7 °C and the temperature of other walls 26.5 °C. The height of the air supply inlet on the top left was 18 mm. The supply air temperature was 22.2 °C and the supply air velocity 1.36 m/s. The outlet height on the bottom right was 24 mm. There were ten monitoring positions as shown in Figure 10(c). On each position, 16 points were measured. The first point was at 0.076 m from the floor. And then a monitor point was set every 0.152 m. We only selected 3 typical positions for comparison. They were P1, P6, and P10. P1 was closest to the inlet, where the forced convection had the strongest effect. P6 was located in the middle of the room, where jet decayed and the forced convection was moderate. P10 was located at the jet end, where forced convection was the weakest, and buoyancy was dominant.

Figure 14 shows the profiles of dimensionless velocity at the 3 positions. At the inertial force dominated position P1, the velocity prediction changed little regardless the wall Prandtl number used that was easy to understand. NWF should behave like SWF and it was indeed. At P6, SWF overestimated the velocity at the bottom; MWF seems slightly better; and NWF improved further. At P10 where natural convection was dominant, the predicted velocities of SWF and MWF were larger than the experimental data. Due to stronger buoyancy effect, NWF did a good job in prediction the velocity in the lower part of P10. The stronger the natural convection was, the better NWF would perform.

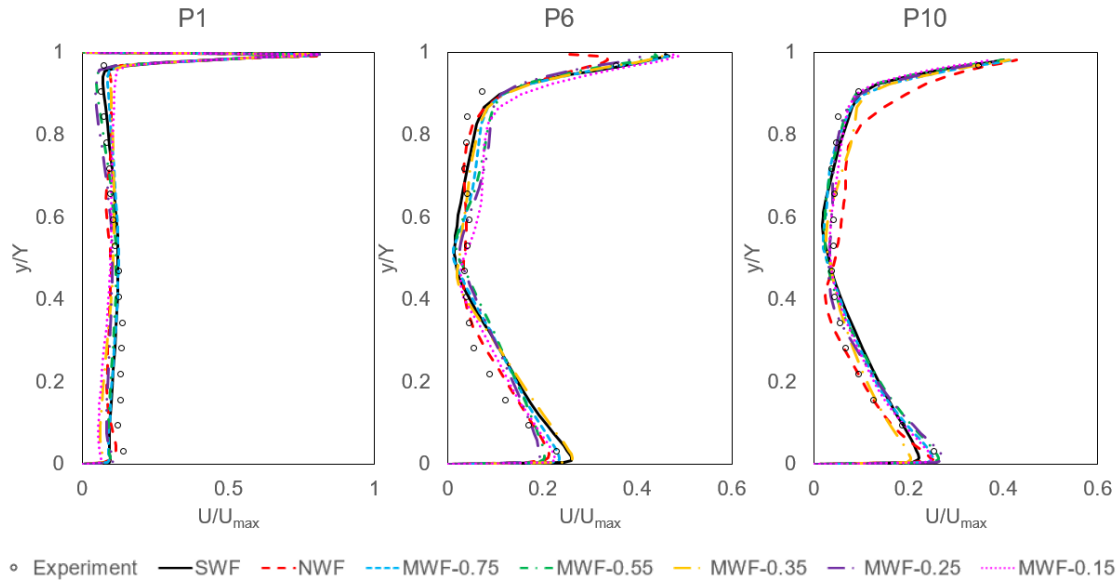

Figure 14. Comparison of the profile of dimensionless velocity at the three positions

Figure 15 compares the predicted profiles of dimensionless air temperature with the experimental data at the 3 positions. At P1 where forced convection was dominated, the predicted temperature by SWF was accurate enough. MWF was poorer than SWF especially when the Prandtl number decreased. NWF did not perform well on this location. At P6 and P10 where the buoyancy force became larger, the predicted temperature by SWF was lower than the experimental data. NWF gave acceptable results. MWF-0.25 performed best at P6 while MWF-0.35 performed best at P10.

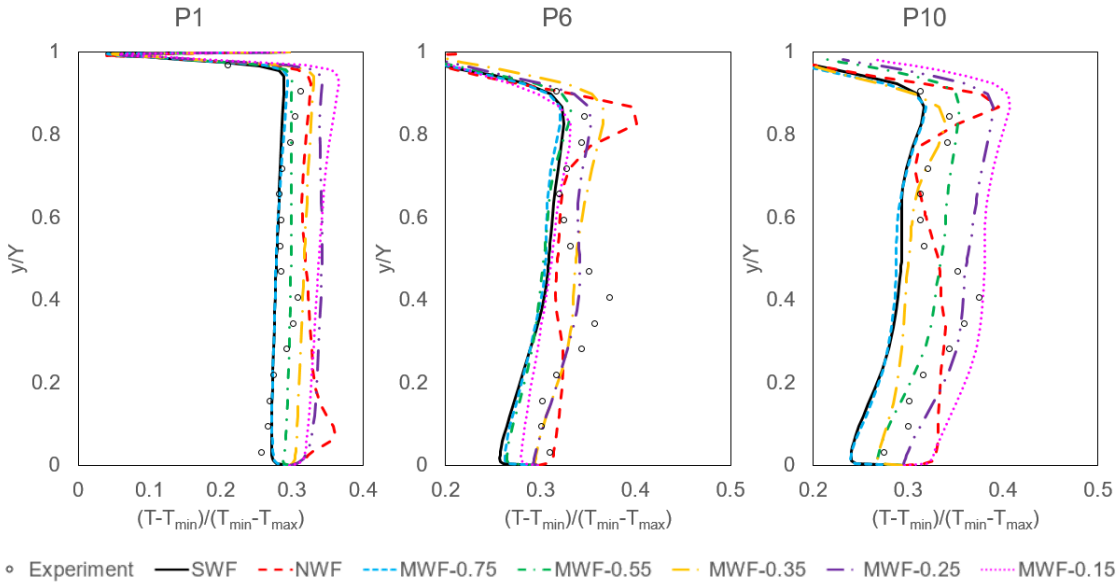

Figure 15. Comparison of the profiles of dimensionless air temperature at the 3 positions

Table 6 showed the RMSE of the dimensionless velocity and temperature for the three wall functions at the P1, P6 and P10. NWF improved the velocity and temperature prediction at P6 and P10. The RMSE of air temperature by NWF was the lowest at the two positions.

Table 6 RMSE of the dimensionless velocity and temperature in three-dimensional case

	P1		P6		P10	
	Velocity	Temperature	Velocity	Temperature	Velocity	Temperature
SWF	0.0322	0.0245	0.0268	0.0532	0.0500	0.0522
NWF	0.0355	0.0452	0.0219	0.0283	0.0205	0.0287
MWF-0.75	0.0315	0.0178	0.0307	0.0380	0.0296	0.0478
MWF-0.55	0.0280	0.0196	0.0347	0.0373	0.0415	0.0412
MWF-0.35	0.0453	0.0357	0.0333	0.0260	0.0331	0.0366
MWF-0.25	0.0332	0.0538	0.0346	0.0188	0.0332	0.0536
MWF-0.15	0.0520	0.0567	0.0361	0.0318	0.0406	0.0703

The above comparisons illustrate that NWF could improve the simulation accuracy for two-dimensional mixed convection. However, NWF could only improve the prediction accuracy in

the regions in the three-dimensional case where buoyancy force dominated. This was because NWF was developed from two-dimensional flow and assumed that the flow feature on the third direction was the same as the other wall direction. The assumption may not be true in many three-dimensional flows.

4. Discussion

The above results show that NWF did not perform well in predicting turbulence kinetic energy. One reason was that the NWF was only for air velocity and temperature not for turbulence energy and its dissipation rate. To improve the NWF further for predicting turbulence parameters, the corresponding wall functions should be developed.

Although the authors have conducted a comprehensive literature review, very few experimental studies were dedicated to high Ra number flow. Quality data of heat transfer near a wall was very rare. Therefore, the cases selected in this study were not ideal. In many cases, we had to use air velocity and temperature profiles of measured data to assess the performance of the new wall function. Despite the fact that wall heat transfer would have an impact on the profile, it is secondary.

This study used standard k-ε model that worked pretty good for many indoor airflows. The model is definitely not the best. Some recommended to improve the model through the simple gradient diffusion hypothesis (SGDH) [33], generalized gradient diffusion hypothesis (GGDH) [34] and Peng, Davidson and Holmberg model (PDH)[35]. Those effort can change the high-Reynolds model to the low-Reynolds models where the flows studied had rather low Reynolds number.

5. Conclusion

The standard wall function could not predict correctly heat transfer on an interior surface of a building, because buoyancy effect was neglected. This paper developed a new wall function to consider the buoyancy effect. The new wall function had an empirical coefficient that is a function of Ri number and can be determined through empirical fit of several flows with buoyancy effect. Thus, the accuracy of the new wall function depends on experimental data of the indoor airflows selected. By applying the new wall function to predict air velocity, temperature and heat transfer in cavities with natural and mixed convection, the study led to the following conclusions.

1) The new wall function can predict air velocity and temperature distribution as well as heat transfer on an interior wall with good accuracy. The performance of the new wall function is much better than the standard wall function and the modified wall function through the near-wall Prandtl number.
2) The new wall function can correctly predict the air temperature gradient near a surface. The new wall function may not be able to calculate accurately turbulence quantities near the surface because the wall functions for turbulence parameters were yet developed. For natural convection, the new wall function could not improve the prediction of air velocity

profile on the outer layer of a wall, which seems to be governed by turbulence model used.

3) The new wall function is proven to be a great alternative to the standard wall function for the range of Ra number studied. The new wall function is also much better than ad hoc modification of near wall Prandtl number presented in the literature.

ACKNOWLEDGEMENT

REFERENCES

1. Obyn, S. and G. Van Moeseke, *Variability and impact of internal surfaces convective heat transfer coefficients in the thermal evaluation of office buildings.* Applied Thermal Engineering, 2015. **87**: p. 258-272.
2. Fisher, D.E. and C.O. Pedersen, *Convective heat transfer in building energy and thermal load calculations*. 1997, American Society of Heating, Refrigerating and Air-Conditioning Engineers ….
3. Zhai, Z.J., et al., *Evaluation of various turbulence models in predicting airflow and turbulence in enclosed environments by CFD: Part 1—Summary of prevalent turbulence models.* Hvac&R Research, 2007. **13**(6): p. 853-870.
4. Zhang, Z., et al., *Evaluation of various turbulence models in predicting airflow and turbulence in enclosed environments by CFD: Part 2—Comparison with experimental data from literature.* Hvac&R Research, 2007. **13**(6): p. 871-886.
5. Launder, B. and D. Spalding, *The numerical computation of turbulent flows. Computer Methods in Applied Mechanics and Energy, 3, 269-289*. 1974.
6. Craft, T., et al., *Progress in the generalization of wall-function treatments.* International Journal of Heat and Fluid Flow, 2002. **23**(2): p. 148-160.
7. Blay, D., S. Mergui, and C. Niculae, *Confined turbulent mixed convection in the presence of a horizontal buoyant wall jet, // ASME HTD - Vol. 213, fundamentals of Mixed Convection.* 1992.
8. Peng, S.-H. and L. Davidson, *Computation of turbulent buoyant flows in enclosures with low-Reynolds-number k-ω models.* International Journal of heat and fluid flow, 1999. **20**(2): p. 172-184.
9. Davidson, L., *Calculation of the turbulent buoyancy-driven flow in a rectangular cavity using an efficient solver and two different low Reynolds number κ-ε turbulence models.* Numerical Heat Transfer, 1990. **18**(2): p. 129-147.
10. Murakami, S., et al., *New low-Reynolds-number k-ε model including damping effect due to buoyancy in a stratified flow field.* International journal of heat and mass transfer, 1996. **39**(16): p. 3483-3496.
11. Henkes, R. and C. Hoogendoorn, *Comparison of turbulence models for the natural convection boundary layer along a heated vertical plate.* International journal of heat and mass transfer, 1989. **32**(1): p. 157-169.
12. Patankar, S.V. and D.B. Spalding, *Heat and mass transfer in boundary layers*. 1968: Morgan-Grampian.
13. Awbi, H.B., *Calculation of convective heat transfer coefficients of room surfaces for natural convection.* Energy and buildings, 1998. **28**(2): p. 219-227.
14. Craft, T., et al., *A new wall function strategy for complex turbulent flows.* Numerical Heat Transfer, Part B: Fundamentals, 2004. **45**(4): p. 301-318.
15. Zhai, Z. and Q.Y. Chen, *Numerical determination and treatment of convective heat transfer coefficient in the coupled building energy and CFD simulation.* Building and Environment, 2004. **39**(8): p. 1001-1009.
16. Wang, H.-Q., et al., *Fume transports in a high rise industrial welding hall with displacement ventilation*

system and individual ventilation units. Building and Environment, 2012. **52**: p. 119-128.

17. Tanasić, N., G. Jankes, and H. Skistad, *CFD analysis and airflow measurements to approach large industrial halls energy efficiency: A case study of a cardboard mill hall.* Energy and Buildings, 2011. **43**(6): p. 1200-1206.
18. Rohdin, P. and B. Moshfegh, *Numerical modelling of industrial indoor environments: A comparison between different turbulence models and supply systems supported by field measurements.* Building and Environment, 2011. **46**(11): p. 2365-2374.
19. Meng, X., et al., *Influence of radiation on predictive accuracy in numerical simulations of the thermal environment in industrial buildings with buoyancy-driven natural ventilation.* Applied Thermal Engineering, 2016. **96**: p. 473-480.
20. Dong, L., et al., *Simulation of heavy gas dispersion in a large indoor space using CFD model.* Journal of Loss Prevention in the Process Industries, 2017. **46**: p. 1-12.
21. Zhang, T.T., H. Zhou, and S. Wang, *An adjustment to the standard temperature wall function for CFD modeling of indoor convective heat transfer.* Building and environment, 2013. **68**: p. 159-169.
22. Cao, J., et al., *Establishment of an improved heat transfer model based on an enhanced thermal wall function for internal combustion engines operated under different combustion modes.* Energy Conversion and Management, 2019. **195**: p. 748-759.
23. Han, Z. and R.D. Reitz, *A temperature wall function formulation for variable-density turbulent flows with application to engine convective heat transfer modeling.* International journal of heat and mass transfer, 1997. **40**(3): p. 613-625.
24. Rakopoulos, C.D., G.M. Kosmadakis, and E.G. Pariotis, *Critical evaluation of current heat transfer models used in CFD in-cylinder engine simulations and establishment of a comprehensive wall-function formulation.* Applied Energy, 2010. **87**(5): p. 1612-1630.
25. Berni, F., G. Cicalese, and S. Fontanesi, *A modified thermal wall function for the estimation of gas-to-wall heat fluxes in CFD in-cylinder simulations of high performance spark-ignition engines.* Applied Thermal Engineering, 2017. **115**: p. 1045-1062.
26. Ng, C., D. Chung, and A. Ooi, *Turbulent natural convection scaling in a vertical channel.* International journal of heat and fluid flow, 2013. **44**: p. 554-562.
27. Kiš, P. and H. Herwig, *The near wall physics and wall functions for turbulent natural convection.* International journal of heat and mass transfer, 2012. **55**(9-10): p. 2625-2635.
28. Tian, Y. and T. Karayiannis, *Low turbulence natural convection in an air filled square cavity: part I: the thermal and fluid flow fields.* International Journal of Heat and Mass Transfer, 2000. **43**(6): p. 849-866.
29. Tian, Y. and T. Karayiannis, *Low turbulence natural convection in an air filled square cavity: Part II: the turbulence quantities.* International Journal of Heat and Mass Transfer, 2000. **43**(6): p. 867-884.
30. Cheesewright, R., K.J. King, and S. Ziai. *Experimental Data for the Validation of Computer Codes for the Prediction of Two-Dimensional Buoyant Cavity Flows, in Significant Questions in Buoyance Affected Enclosure or Cavity Flows*. in *ASME*. 1986.
31. George Jr, W.K. and S.P. Capp, *A theory for natural convection turbulent boundary layers next to heated vertical surfaces.* International Journal of Heat and Mass Transfer, 1979. **22**(6): p. 813-826.
32. Wang, M. and Q. Chen, *Assessment of various turbulence models for transitional flows in an enclosed environment (RP-1271).* Hvac&r Research, 2009. **15**(6): p. 1099-1119.
33. Yan, Z. and G. Holmstedt, *A two-equation turbulence model and its application to a buoyant diffusion flame.* International Journal of Heat and Mass Transfer, 1999. **42**(7): p. 1305-1315.
34. Ince, N. and B. Launder, *On the computation of buoyancy-driven turbulent flows in rectangular*

enclosures. International Journal of Heat and Fluid Flow, 1989. **10**(2): p. 110-117.

35. Peng, S.-H., L. Davidson, and S. Holmberg, *A modified low-Reynolds-number k-ω model for recirculating flows.* 1997.

36. Kumar, R. and A. Dewan, *URANS computations with buoyancy corrected turbulence models for turbulent thermal plume.* International Journal of Heat and Mass Transfer, 2014. **72**: p. 680-689.